Remote Image Fusion Based on PCA and Dual Tree Compactly Supported Shearlet Transform

Chang Duan

School of Electronic Engineering,Research Institute of Electronic Science and Technology
University of Electronic Science and Technology
Qingshuihe Campus:No.2006, Xiyuan Ave, West Hi-Tech Zone, Chengdu, Sichuan, P.R.China
pertinax@163.com

Qi Hong Huang

Electronic Engineering College
Chengdu University of Information Technology
No. 24 Xuefu Road Southwest Airport Economic Development Zone, Chengdu, Sichuan , P.R.China
y97hqh@cuit.edu.cn

Xue Gang Wang and Shuai Wang

School of Electronic Engineering
University of Electronic Science and Technology
Qingshuihe Campus:No.2006, Xiyuan Ave, West Hi-Tech Zone, Chengdu, Sichuan, P.R.China
xgwang@ee.uestc.edu.cn; wangshuai0601@gmail.com

ABSTRACT. *This paper presents a novel remote sensing image fusion algorithm, which implements panchromatic sharpening of multispectral data through application of the principal component analysis (PCA) transform and the dual-tree compactly supported shearlet transform (DT CSST). Shearlet transforms provide near optimal representation of the anisotropic features of an image. The compactly supported shearlet transform (CSST) as the spatial domain implementation of discrete shearlet transform may represent the directions by the way of dilation operations directly in spatial domain. Since most of the prominent features of images, such as edges and regions, have finite regions in spatial domain, CSST is very suitable for image fusion. However, the conventional CSST, which is shift-variant, causes distortions in fused images. With the embedded structure of dual-tree (DT) in the CSST, the shift-variant properties can be effectively reduced. The evaluation results of experiments indicated that the proposed method is superior to other PCA and multi-scale transform based methods such as curvelet, band limited shearlet transform (BLST), which is an invariant shearlet transform,à trous wavelet transform, the dual-tree complex wave transform (DTCWT), and the discrete wavelet transform (DWT).*

Keywords:compactly supported shearlet transform, panchromatic multispectral image fusion, Pan-sharpening, Dual-tree

1. **Introduction.** Different image sensors are equipted on satellites to capture different images of the same area or object. Usually different images contain different features of the area or object. Two types of images can be found on a satellite: panchromatic images, which record the total intensity of radiation falling on each pixel, and multispectral images, which record the intensity of radiation in a small band of visible spectra, such as ranging from 0.7 μm to 0.4 μm, called the red-green-blue (RGB) region, and infrared

spectra, where wavelengths is from 0.7 μm to 10 μm or greater are classified as either near infrared (NIR), middle infrared (MIR), or far infrared (FIR or thermal). Panchromatic images supply high spatial resolution for distinguishing features, while multispectral images supply high spectral resolution. In many applications, it would be more helpful if images had both high spatial and high spectral resolutions. This has led to development of the panchromatic and multispectral image fusion algorithm.

The panchromatic and multispectral image fusion algorithm, or Pan-sharpening technique, has been studied for decades. In the early period of this research, the fused images were simply a linear combination of source images, such as Brovery Transform [1]. These early methods are simple, but the quality of fused images is low. Later, researchers realized that colour information is actually useful and should be maintained. Thus, many solutions in colour space have been proposed, and the representative methods are IHS [2] and principal component analysis (PCA) [3] algorithms, in which a main spectral component is generated from multispectral images, and this main component will be substituted by panchromatic images to increase the spatial resolution prior to inverse IHS or PCA transform. By this procedure, spatial resolution is increased and the spectral information is maintained as much as possible. Gradually, researchers realized that both the spatial and spectral consistencies should be maintained simultaneously. With the development of harmonic analysis theory, several multi-scale transform-based methods have been proposed, include the DWT [3], the à trous wavelet transform [4], the dual-tree complex wavelet transform [5, 6], and the curvelet [7, 8]. Many of these methods combined IHS or PCA simultaneously.

Among the multi-scale transforms, the shearlet system stands out in recent years for its efficient representation of multidimensional data. Indeed, many other transforms have been introduced to overcome the limitation of traditional multi-scale methods which do not capture edges and other anisotropic features in a satisfactory manner. The shearlet transform has many advantages. For example, it is unique in that it has a single or finite set of generating functions; it provides almost optimal representations for multi-dimensional data; it allows a unified treatment of the continuum and digital realms, and it provides a compactly supported transform. Presently, there are two categories of the implementation of the discrete shearlet transform: Fourier-domain based approaches and spatial-domain based approaches. The Fourier-domain based approaches have better frequency localization, while the spatial-domain based approaches have better spatial localization. According to the Uncertainly Principle, the product of $S_F \times S_S$ is a constant, where S_F and S_S represent the size of frequency and spatial windows respectively, meaning that increasing or decreasing both S_F and S_S simultaneously is impossible. In the case of image fusion, spatial localization is more important than frequency localization because most of the prominent features of images, such as the regions and edges, have limited region in the spatial domain, and the human visual system also extracts that information directly from the spatial domain. The compactly supported shearlet transform (CSST) belongs to the spatial-domain based implementation category [9, 10]. However, CSST has a shift-variant disadvantage to image fusion because it is based on a traditional critically-sampled discrete wavelet transform. Fortunately, this disadvantage can be sophisticatedly mitigated by the dual-tree structure, the details of which will be discussed in Section 3.

Many image fusion methods based on the shearlet transform have been proposed recently. A remote sensing image fusion method based on the band-limited shearlet transform (BLST) has been proposed by Chai et al in [11] , and claimed to be superior to the curvelet method. Miao [12, 13] discussed the multi-focus image fusion method based on the CSST, but the shift-variant property of the CSST was not considered and, consequently, no compensation was made for it. Deng [14] proposed an IHS and shearlet-based

panchromatic and multispectral image fusion method, but did not clearly describe which type of shearlet implementation was used.

In this paper, the dual-tree compactly supported shearlet transform (DT CSST) [15], which is almost shift-invariant, is reported firstly. Then, a panchromatic multispectral image fusion method based on PCA and DT CSST is proposed. The PCA guarantees the spectral consistency as well as the DT CSST provides the ability to extract spatial information from the panchromatic image. The rest of the paper is organized as described in the following sentences. The basic theory of the shearlet transform and its digital implementation of CSST are introduced in Section 2. The construction of DT CSST and its shift invariant property are introduced in Section 3. The proposed remote image fusion method is given in Section 4. After the experiments and analysis in Section 5, conclusions are drawn in Section 6.

2. **Compactly Supported Shearlet Transform.** In this section, the basic theory of the shearlet transform and the implementations of CSST are briefly introduced. A shearlet transform is a special case of the composite dilation wavelet transform. The dilation operation D_M is given as:

$$D_M \psi(x) = |det M|^{-1/2} \psi(M^{-1}x), M \in GD_d(\mathbb{R}), \tag{2.1}$$

where M is the parameter of the dilation operation, $\psi(x)$ is any function, and $GD_d(\mathbb{R})$ represents the group of d-dimensional invertible matrices defined on $\mathbb{R}$. The translation operation T_t is given as:

$$T_t \psi(x) = \psi(x - t), t \in \mathbb{R}. \tag{2.2}$$

Let $A = \begin{pmatrix} a & 0 \\ 0 & a^{1/2} \end{pmatrix}$, $a > 0$ be the parabolic scaling matrices, and $S = \begin{pmatrix} 1 & s \\ 0 & 1 \end{pmatrix}$, $s \in \mathbb{R}$ be the shearing matrix. The continuous shearlet system $SH(\psi), \psi \in L^2(\mathbb{R}^2)$ is defined by:

$$SH(\psi) = \{\psi_{a,s,t} = T_t D_{A_a} D_s \psi : a > 0, s \in \mathbb{R}, t \in \mathbb{R}^2\}. \tag{2.3}$$

The definition of the continuous shearlet transform of $f \in L^2(\mathbb{R}^2)$ is the mapping:

$$f \mapsto SH_\psi f(a, s, t) = < f, \sigma(a, s, t)\psi >, (a, s, t) \in \mathbb{S}, \tag{2.4}$$

where $\mathbb{S} : (\mathbb{R}^+ \times \mathbb{R}) \times \mathbb{R}^2$, $\sigma(a, s, t)\psi = T_t D_{A_a} D_{S_s}\psi$. The irregular discrete shearlet system upon ψ and Λ is $DSH(\psi, \Lambda) = \{\psi_{a,s,t} = a^{-3/4}\psi(A_a^{-1}S_s^{-1}(. - t)) : (a, s, t) \in \Lambda\}$. A (regular) discrete shearlet system associated with ψ, is duplicated with Eq (2.3), is defined by $SH(\psi) = \{\psi_{j,k,m} = 2^{3j/4}\psi(S_k A_{2j}. - m) : j, k \in \mathbb{Z}, m \in \mathbb{Z}^2\}$. Notice that the regular versions of discrete shearlet systems are derived from irregular systems by choosing $\Lambda = \{(2^{-j}, -k, S_{-k}A_{2^{-j}}m) : j, k \notin \mathbb{Z}, m \in \mathbb{Z}^2\}$. The discrete shearlet transform of $f \in L^2(\mathbb{R}^2)$ is the mapping defined by:

$$f \mapsto DSH_\psi f(j, k, m) = < f, \psi_{j,k,m} >, (j, k, m) \in \mathbb{Z} \times \mathbb{Z} \times \mathbb{Z}^2 \tag{2.5}$$

Cone-adapted shearlets were introduced for the purpose of treating the different directions more equally, so the number of directions could be limited [16]. In the study by Lim [9], the principles and the details of the construction of the CSST were presented, including separable and non-separable transforms. The forward and backward steps of the CSST are given in Fig.1. The input function $f(x)$ is firstly processed by dilation operations in vertical and horizontal cones directly in the spatial domain. Then, the anisotropic discrete wavelet transform (ADWT) is performed on every sheared version of the input signal. The outputs of ADWT, $C_{j,1,m}, \dots, C_{j,k,m}$ and $\tilde{C}_{j,1,m}, \dots \tilde{C}_{j,k,m}$ are the coefficients of both cones, where the parameter k is the number of directions in each cone.
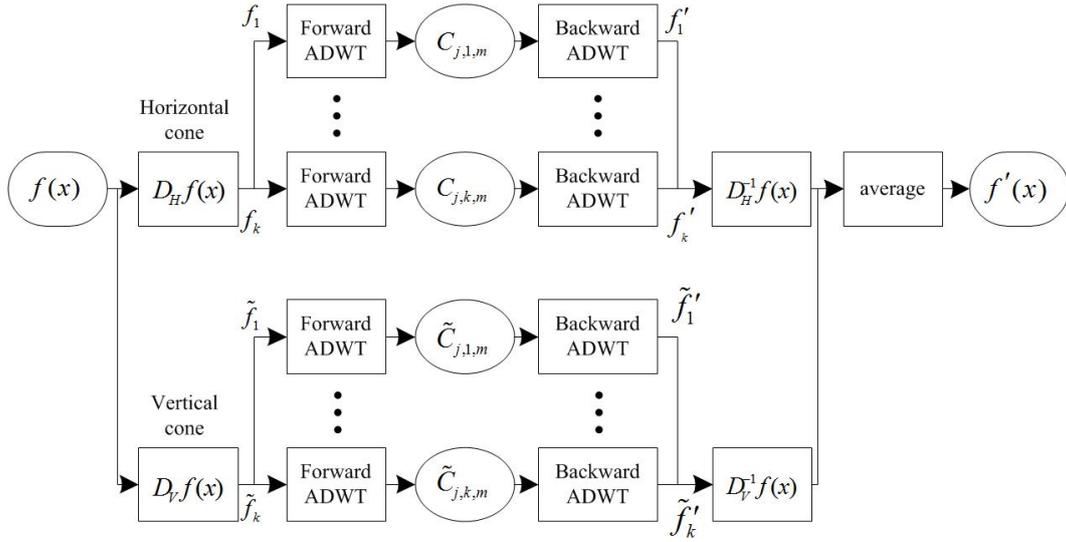
FIGURE 1. Forward and backward CSST

3. **Dual Tree Compactly Supported Shearlet Transform.** The dual-tree complex [17, 18] wavelet transform employs two real discrete wavelet transforms (DWTs). The first DWT gives the real part of the transform, while the second DWT gives the imaginary part. The two real wavelet transforms use two different sets of filters, each of which satisfy the PR (Perfect Reconstruction) conditions separately. The two sets of filters are jointly designed so that the overall transform is approximately analytic. If these two DWTs satisfy the half-sample delay condition, which indicates that the wavelets form an approximate Hilbert transform pair, the transform would be approximately shift-invariant. Heuristically, the definitions of forward DT CSST can be represented as follows:

Let $CS_{\psi\varphi}f(j,s,k)$ represents the DT CSST for f, and its coefficients are calculated by:

$$CS_{\psi\varphi}f(j,s,k) = SH_\psi f(j,s,k) + jSH_\varphi f(j,s,k), \qquad (3.1)$$

where $SH_\psi f(j,s,k)$ and $SH_\varphi f(j,s,k)$ denote the real and imaginary parts of the complex coefficients, which can be calculated by equation (2.4). The backward DT CSST transform or reconstruction of f is given by:

$$\tilde{f}(x) = \frac{1}{2}\sum_{j,s\in\mathbb{Z}, k\in\mathbb{Z}^2} <f,\psi_{j,s,k}> \psi_{j,s,k} + \frac{1}{2}\sum_{j,s\in\mathbb{Z}, k\in\mathbb{Z}^2} <f,\varphi_{j,s,k}> \varphi_{j,s,k} \qquad (3.2)$$

This study used the same method in [18, 19]. Kingsbury illustrated the shift-variance of DWT and the shift-invariance of DT CWT. The comparison of reconstruction results, scale-by-scale, for a traditional DT CSST and CSST are given in Fig.2. The input image is a white circle located at the centre of a black background. The top and bottom rows are the reconstruction for the same direction for a horizontal cone of the DT CSST and CSST respectively. It can be observed in Fig.2(a) that both the DT CSST and the CSST can reconstruct the input image precisely. But in various scales, the reconstruction images of DT CSST are much smoother than those of CSST. This comparison shows the shift-variant effect of the CSST and the approximate shift-invariant effect of the DT CSST.

4. **Proposed method and measurements.**

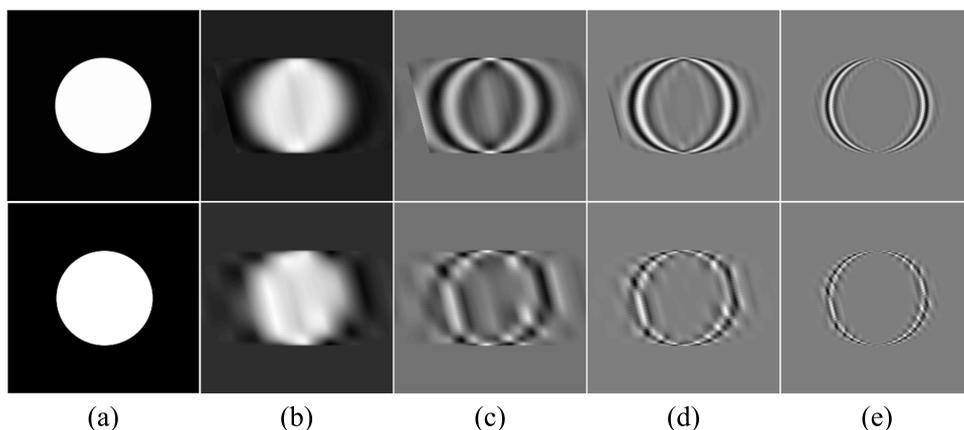(a)   (b)   (c)   (d)   (e)

FIGURE 2. The comparison of reconstruction where the following are represented: (a) the reconstruction of all coefficients, (b) the reconstruction by the low frequency coefficients, (c) to (e) the reconstructions by each different single scales of high frequency coefficients.

4.1. General Multi Resolution Framework for Image Fusion.

General Multi Resolution Framework (GMRF) for image fusion, in this paper, refers to steps in Fig.3. The letters A and B represent two input images, and they are decomposed by certain forward transforms into two sets of coefficients, denoted by C_A and C_B. Then, under certain fusion rules, these coefficients are fused into one set, which is denoted by C_F. Finally, the output image P_{GMRF} is produced by the inverse transform upon C_F. It is a simplified version of the framework of [21]. This simplification is conducted because the classic framework emphasize the competition of the salient information of different source images, while in this manuscript there's no competition of different source information. The coefficients of C_A and C_B, which are decomposed by DT CSST from source images, have different features: C_A is generated from the panchromatic image, which is monochromatic with high spatial resolution and C_B is generated from multispectral images, which is the primary component of multispectral images. In the fusion rule, the high frequency coefficients C_{FH} are extracted from C_{AH} and the low frequency coefficients C_{FL} are the average of both C_{AL} and C_{BL} as given in equation (4.1):

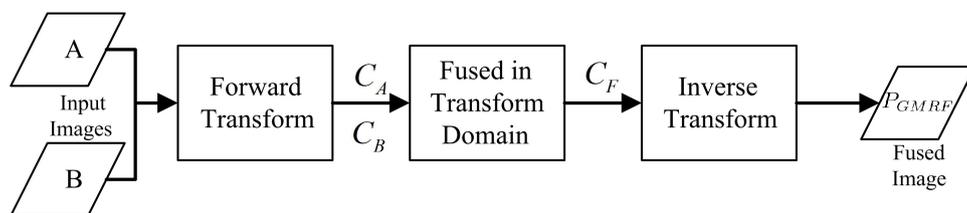$$\begin{cases} C_{FL} = mean(C_{AL} + C_{BL}) \\ C_{FH} = C_{AH} \end{cases} . \tag{4.1}$$

FIGURE 3. General Multi Resolution Framework (GMRF) for image fusion

4.2. Principal component analysis.

Principal component analysis (PCA) is a mathematical procedure which transforms a number of potentially correlated variables into a smaller number of uncorrelated variables called principal components. The objective of

PCA is to reduce the dimensionality (the number of variables) of the dataset while retaining most of the original variability in the data. The first principal component accounts for the most of the variability in the data, and each succeeding component accounts for as much of the remaining variability as possible. Thus, PCA is concerned with explaining the variance and covariance structure of a high-dimensional random vector through a few linear combinations of the original component variables. PCA is also named as discrete Karhunen-Loeve transform (KLT) [20]. A common way to find the principal components of a data set is by calculating the eigenvectors of the data covariance matrix. These eigenvectors give the directions in which the data distribution is stretched most. The projections of the data on the eigenvectors are the principal components. The corresponding eigenvalues give an indication of the amount of information represented by the respective principal components.

The classic fusion method based on PCA can be written in equation(4.2) and (4.3), where the matrix $\{v_{ii}\}$ represents the PCA transform matrix. The primary component of multi-spectral image is substituted by the histogram equalized panchromatic image P_{HE}. And the drawback of this type method is excessive spatial information is injected into the fused images, consequently reduce the spectral consistency.

$$\begin{pmatrix} C_1 \\ C_2 \\ ... \\ C_n \end{pmatrix} = \begin{pmatrix} v_{11} & v_{21} & ... & v_{n1} \\ v_{12} & v_{22} & ... & v_{n2} \\ ... & ... & ... & ... \\ v_{1n} & v_{2n} & ... & v_{nn} \end{pmatrix} \begin{pmatrix} MS_1 \\ MS_2 \\ ... \\ MS_n \end{pmatrix} \tag{4.2}$$

$$\begin{pmatrix} F_1 \\ F_2 \\ ... \\ F_n \end{pmatrix} = \begin{pmatrix} v_{11} & v_{12} & ... & v_{1n} \\ v_{21} & v_{22} & ... & v_{2n} \\ ... & ... & ... & ... \\ v_{n1} & v_{n2} & ... & v_{nn} \end{pmatrix} \begin{pmatrix} P_{HE} \\ C_2 \\ ... \\ C_n \end{pmatrix} \tag{4.3}$$
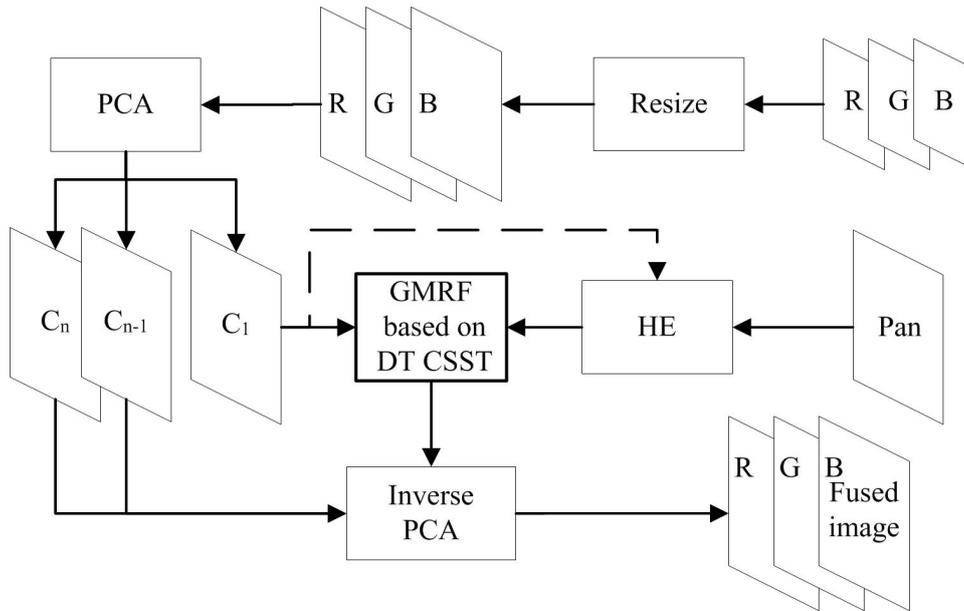

FIGURE 4. the steps of proposed method

4.3. **Main frame of the proposed method.** The main frame of the proposed method is given in Fig.4. Firstly, the small-sized multispectral images are resized to the same size

as the panchromatic image, and the PCA transform is performed on the resized multi-spectral images. The outputs are various composition components. Then, the histogram equalization (HE) operation is performed on the panchromatic image according to the grey-scale distribution of the primary component of the multispectral images (C_1). This step can make the substituting panchromatic image closer to that of the multispectral images in order to retain more spectral consistency. GMRF based on the DT CSST is performed in the next step. Finally, the inverse PCA transform is performed, and the result is the final fused image. The difference of the proposed method and the classical PCA method is the substituting component is the result of GMRF with DT CSST (P_{GMRF}) instead of P_{HE}, as in equation(4.4). By tuning the scale parameter of DT CSST, the amount of spatial information from panchromatic image can be adjusted meanwhile modified the spatial consistency and spectral consistency of the fused image. The proposed method still belongs to the general image fusion methods in [22], the innovation is taking the advantage of DT CSST, which has a better ability to capture anisotropic features of panchromatic image.

$$
\begin{pmatrix} F_1 \\ F_2 \\ ... \\ F_n \end{pmatrix} = \begin{pmatrix} v_{11} & v_{12} & ... & v_{1n} \\ v_{21} & v_{22} & ... & v_{2n} \\ ... & ... & ... & ... \\ v_{n1} & v_{n2} & ... & v_{nn} \end{pmatrix} \begin{pmatrix} P_{GMRF} \\ C_2 \\ ... \\ C_n \end{pmatrix} \tag{4.4}
$$

4.4. **performance measurements.** Three space consistency and three spectral consistency indices are selected to analyse the methods objective performance. Space consistency indices include mutual information MI,$Q^{AB|F}$ (represented later by Q) [19] and Q0 [23]. Spectral consistency indices incude $RASE$, $ERGAS$ and $Q3$ of [2].

MI measures how much information, which originated in the source images, is contained in the fused image. It is defined as:

$$
MI = I_{FA} + I_{FB} \tag{4.5}
$$

where $I_{FT}(f,t) = \sum_{f,t} P_{FT} log \frac{P_{FT}(f,t)}{P_F(f)P_T(t)}, T \in \{A,B\}, t \in \{a,b\}$, and P is the distribution of grey-scale of images.

Q evaluates the amount of edge information that is transferred from the input images to the output fused images. Larger value of Q means more amount of important edge information is being transferred from panchromatic images to fused images.

The index $Q0$ in [24], is defined as:

$$
Q0 = \frac{4\sigma_{xy}\overline{(xy)}}{(\bar{x}^2 + \bar{y}^2)(\sigma_x^2 + \sigma_y^2)} \tag{4.6}
$$

which can be decomposd as:

$$
Q0 = \frac{\sigma_{xy}}{\sigma_x\sigma_y} \cdot \frac{2\bar{x}\bar{y}}{\bar{x}^2\bar{y}^2} \cdot \frac{2\sigma_x + \sigma_y}{\sigma_x^2 + \sigma_y^2} \tag{4.7}
$$

where x and y denote two input images, $\bar{x}$ and $\bar{y}$ are the mean of x and y, σ_x^2 and σ_{xy} denote the variance of x and the covariance of x, y. The value of $Q0$ is between -1 and 1. The maximum value of 1 is achieved when x and y are identical.

$RASE$ is defined as (4.8), can estimate the average performance of the method of image fusion in the spectral bands.

$$
RASE = \frac{100}{M} \sqrt{\frac{1}{N} \sum_{i=1}^{N} RMSE^2(B_i)}, \tag{4.8}
$$

where N is the number of multispectral images, M is the mean radiance of all multispectral images, B_i is each multispectral image, $RMSE$ is the root mean square error defined as: $RMSE^2(B_i) = bias^2(B_i) + SD^2(B_i)$.

$ERGAS$ refers to the relative global dimensional synthesis error:

$$ERGAS = 100\frac{h}{l}\sqrt{\frac{1}{N}\sum_{i-1} N\frac{RMSE^2(B_i)}{M_i^2}} \qquad (4.9)$$

where h is the resolution of the panchromatic image, l is the resolution of the multispectral images, and M_i is the mean radiance of each spectral image. Smaller $RASE$ and $ERGAS$ indicates better spectral consistency between fused images and source images.

Let $\{a_1, b_1, c_1\}$ and $\{a_2, b_2, c_2\}$ denote the three spectral band radiance value of original multispectral and fusion images. Let $z_1 = a_1 + ib_1 + jc_1$ and $z_2 = a_2 + i + b_2 + jc_2$ denote the three-band original multispectral image and the fused image, respectively. Then, $Q3$ is defined as in Equation (4.10).

$$Q3 = \frac{|\sigma_{z_1 z_2}|}{\sigma_{z_1} \cdot \sigma_{z_2}} \cdot \frac{2\sigma_{z_1} \cdot \sigma_{z_2}}{\sigma_{z_1}^2 + \sigma_{z_2}^2} \cdot \frac{2|\bar{z}_1| \cdot |\bar{z}_2|}{|\bar{z}_1|^2 + |\bar{z}_1|^2} \qquad (4.10)$$

where $\sigma_{z_1 z_2}$ is the hyper-complex covariance between z_1 and z_2, σ_{z_1} and σ_{z_2} are the square roots of the variances of z_1 and z_2, $\bar{z}_1$ and $\bar{z}_2$ are the expected values of z_1 and z_2, and $|\cdot|$ is the modulus of $\cdot$. The maximum value, 1, is achieved when z_1 and z_2 are identical.

5. **Experiment.** Three groups of source images are shown in the first and second column in first row from Fig.5 to Fig.7. Group 1 is from QuickBird and Group 2 and Group 3 are from IKONOS. The spatial resolution of QuickBird and IKONOS are 0.6 and 1 m for the panchromatic image and 2.4 and 4 m for the multispectral images. The sizes of all of the panchromatic and multispectral images are 512×512 and 128×128. The multispectral images have been resized to the same size as the panchromatic in Fig.5 to Fig.7.

The proposed DT CSST based method is evaluated as well as other transform based methods, including DWT, DTCWT, À trous wavelet transform, Band limited Shearlet Transform and Curvelet Transform. All the methods are evaluated at all the value of number of scale which determine how many times the transform are performed. Both measurements of spatial and spectral quality indices are evaluated. For the limitation of the paper, only the indices of first group with the scale number from 2 to 5 are listed in Table.1 and Table.2. From the both tables, it should be noticed that although the proposed method and the BLST based method have the largest indices in spatial consistency, but their spectral consistency is not the best. Result images of all three groups with the scale number 5, are shown in Fig.5 to Fig.7.

However, the spatial consistency and spectral consistency are negative correlated. The curves of MI with $RASE$ and MI with $Q3$ for all three groups are shown, the other curves, such as $Q0$ with $RASE$ or Q with $ERGAS$, are similar to the curves in Fig.8, so they are not shown. It should be noticed the curves of proposed method (black lines), are at the most right side. This phenomena indicates in all three groups, if the MI is the same, the proposed method has the least loss in spectral consistency or if the $RASE$ or $Q3$ is the same, the proposed method has the largest MI. This observation clearly suggests that the performances of proposed method are superior to all the other methods. And the recommended scale number is 5, because the performance curves have inflection points near it.
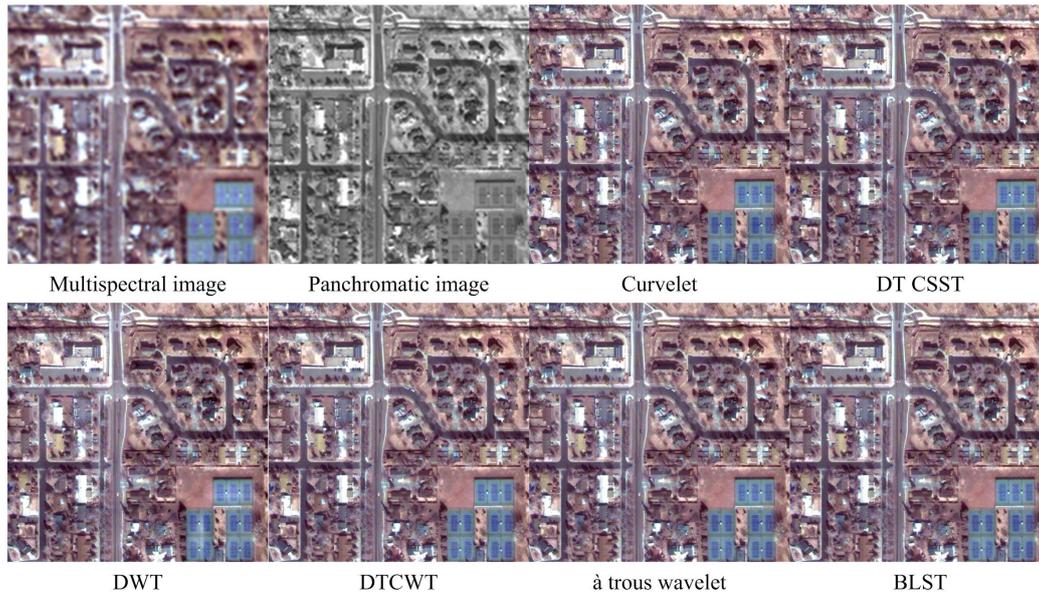
Multispectral image	Panchromatic image	Curvelet	DT CSST
DWT	DTCWT	à trous wavelet	BLST

FIGURE 5. The influence of shift-variant property

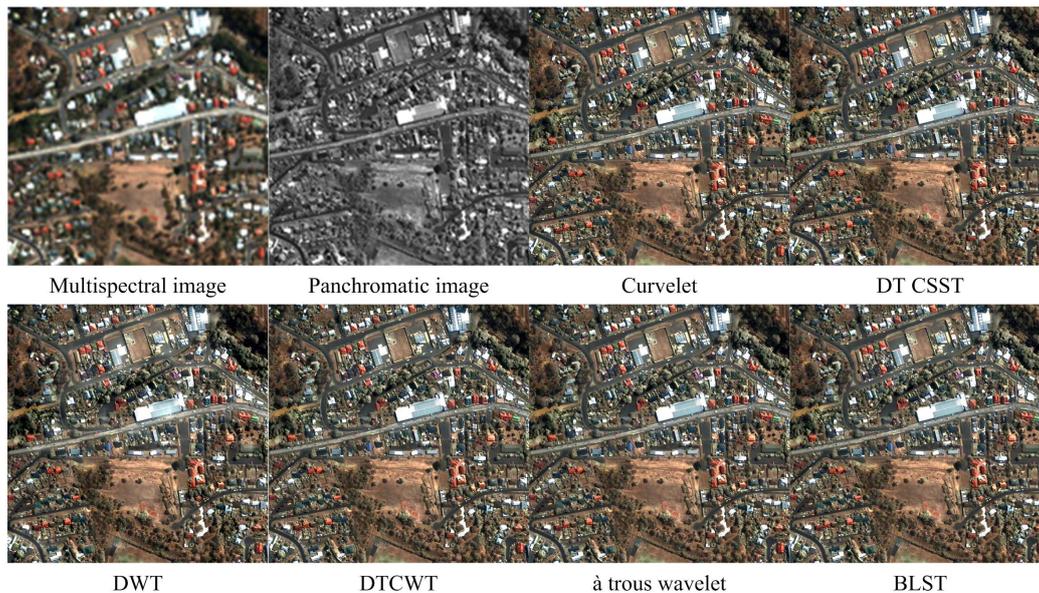|			
Multispectral image	Panchromatic image	Curvelet	DT CSST
DWT	DTCWT	à trous wavelet	BLST

FIGURE 6. source and result images of second group

6. **Conclusion.** Shearlet theory has a better ability to represent anisotropic features of multi-dimensional data than conventional wavelet theory. The advantages of CSST, such as multi-resolution on directions, compactly supported in the spatial domain, make it very suitable for remote image fusion. However, its shift-variant property leads to distortions in fused images and hampers the performance. The dual-tree structure of DT CWT can be embedded here to reduce the shift variant property of conventional CSST. Combining the DT CSST and PCA transforms, the proposed remote image fusion method can effectively fulfil the task of fusing the panchromatic and the multispectral images. According to the experimental results, the proposed remote image fusion method is superior to the methods based on curvelet, BLST, à trous wavelet, DT CWT, and DWT.
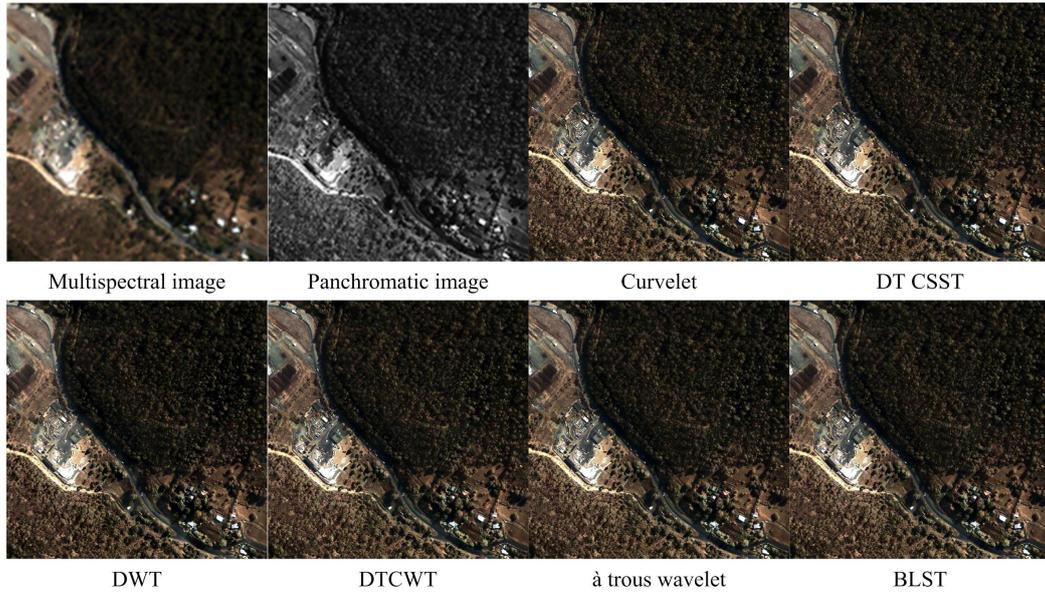
| Multispectral image | Panchromatic image | Curvelet | DT CSST |

| DWT | DTCWT | à trous wavelet | BLST |

FIGURE 7. source and result images of third group

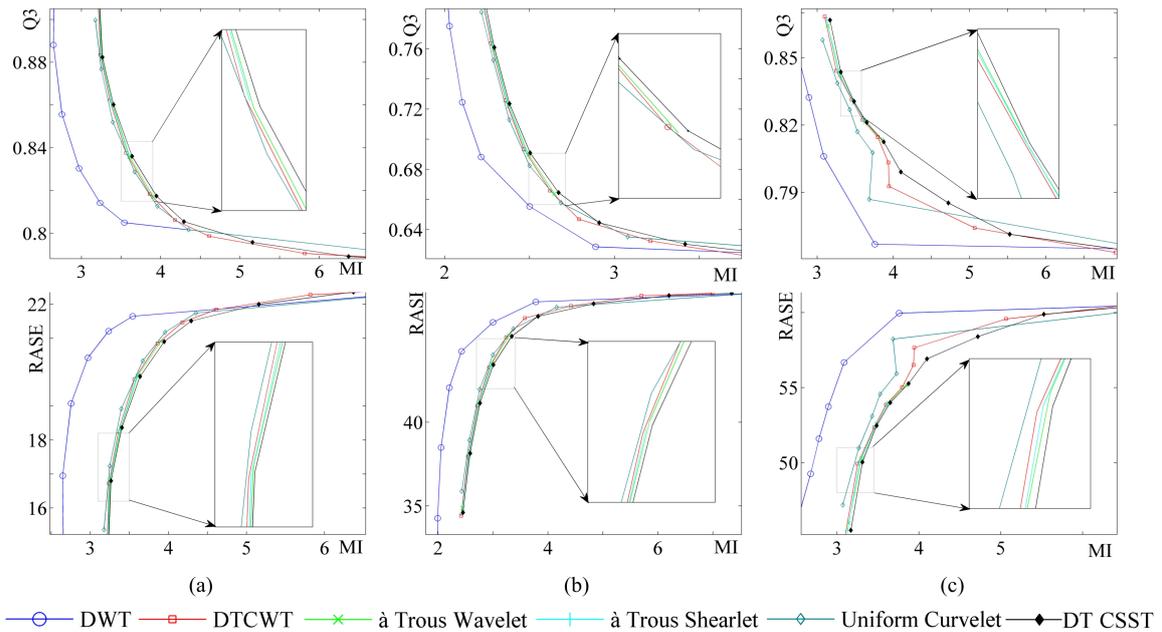DWT ○   DTCWT □   à Trous Wavelet ✕   à Trous Shearlet +   Uniform Curvelet ◇   DT CSST ◆

FIGURE 8. the performance curves for three groups(from left to right are first to third group consequently)

REFERENCES

[1] E. S. Elghazali, Performance of quickbird image and lidar data fusion for 2d/3d city mapping, *Australian Journal of Basic and Applied S ciences*, vol. 5, no. 11, pp. 1588-1600, 2011.

[2] M. Choi, A new intensity-hue-saturation fusion approach to image fusion with a tradeoff parameter, *IEEE Trans. Geoscience and Remote Sensing*, vol. 44, no. 6, pp. 1672-1682, 2006.

TABLE 1. Spatial consistency quality indices of first subjects

Scale	indices	DWT	DT CWT	à trous wavelet	Cuvelet	BLST	DT CSST
2	MI	1.9792	2.4066	2.4292	2.4162	2.4209	2.4384
	Q	0.43197	0.61735	0.63191	0.63375	0.62496	0.63304
	Q0	0.78855	0.94232	0.94543	0.94745	0.94379	0.94533
3	MI	1.98	2.5277	2.559	2.5539	2.5449	2.567
	Q	0.57259	0.6741	0.68036	0.68086	0.67742	0.68018
	Q0	0.85173	0.9585	0.9609	0.96204	0.95965	0.96113
4	MI	2.0421	2.6974	2.7367	2.7395	2.7177	2.7472
	Q	0.64963	0.70038	0.70291	0.70346	0.70175	0.70261
	Q0	0.89607	0.97179	0.97361	0.97475	0.97267	0.97393
5	MI	2.1891	2.9115	2.9654	2.9813	2.9387	2.9885
	Q	0.68941	0.71019	0.71121	0.71139	0.71071	0.71097
	Q0	0.9336	0.98154	0.98311	0.98399	0.98229	0.98348

TABLE 2. Spectral consistency quality indices of first subjects

Scale	indices	DWT	DT CWT	à trous wavelet	Cuvelet	BLST	DT CSST
2	Rase	28.8933	34.4875	34.9395	35.9518	34.6378	34.6802
	Ergas	317.1407	378.5444	383.5053	394.616	380.194	380.6587
	Q3	0.87229	0.79987	0.79565	0.7858	0.7985	0.79813
3	Rase	34.3112	38.0073	38.3565	39.0302	38.1381	38.2339
	Ergas	376.6085	417.1782	421.0113	428.4056	418.6136	419.6652
	Q3	0.82507	0.76544	0.76142	0.75412	0.76388	0.7625
4	Rase	38.5748	41.1101	41.3963	42.0826	41.2069	41.2551
	Ergas	423.4075	451.235	454.3768	461.9095	452.2978	452.8274
	Q3	0.77653	0.72769	0.7238	0.71484	0.72632	0.72541
5	Rase	42.1756	43.4052	43.6348	44.1566	43.4822	43.5579
	Ergas	462.9311	476.4265	478.947	484.6749	477.2724	478.1027
	Q3	0.72631	0.69546	0.69186	0.68457	0.69421	0.69297

[3] M. Gonzlez-Audcana, et al., Fusion of multispectral and panchromatic images using improved IHS and PCA mergers based on wavelet decomposition, *IEEE Trans. Geoscience and Remote Sensing*, vol. 42, no. 6, pp. 1291-1299, 2004.

[4] J. Nunez, et al., Multiresolution-based image fusion with additive wavelet decomposition, *IEEE Trans. Geoscience and Remote Sensing*, vol. 37, no. 3, pp. 1204-1211, 1999.

[5] S. Ioannidou, and V. Karathanassi, Investigation of the dual-tree complex and shift-invariant discrete wavelet transforms on Quickbird image fusion, *IEEEE Geoscience and Remote Sensing Letters*, vol. 4, no. 1, pp. 166-170, 2007.

[6] P. R. Hill, et al., Image fusion using a new framework for complex wavelet transforms, *Proc.of IEEE International Conference Image Processing*, pp. II-1338-41, 2005.

[7] M. Choi, et al., Fusion of multispectral and panchromatic satellite images using the curvelet transform, *IEEE Geoscience and Remote Sensing Letters*, vol. 2, no. 2, pp. 136-140, 2005.

[8] Q. Zhang, and B. l. GUO, Fusion of remote sensing images based on the second generation curvelet transform, *Optics and Precision Engineering*, vol. 7, pp. 1131-1135, 2007.

[9] W. Q. Lim, The discrete shearlet transform: a new directional transform and compactly supported shearlet frames,*IEEE Trans. Image Process*, vol. 19, vol. 5, pp. 1166-80, 2010.

[10] G. Kutyniok and W. Q. Lim, Compactly supported shearlets are optimally sparse, *Journal of Approximation Theory*, vol. 163, no. 11, pp. 1564-1589, 2011.

[11] Y. Chai, et al., Remote sensing image fusion based on iterative discrete Shearlet transform, *Computer Engineering and Applications*, vol. 47, pp. 174-176, 2011.

[12] Q. g. Miao, et al., A novel algorithm of image fusion using shearlets, *Optics Communications*, vol. 284, no. 6, pp. 1540-1547, 2011.

[13] Q. Miao, et al., Multi-focus image fusion algorithm based on shearlets, *Chinese Optics Letters*, vol. 9, no. 4, pp. 041001, 2011.

[14] C. Deng, et al., Remote sensing images fusion algorithm based on shearlet transform, *Proc. of International Conference on Environmental Science and Information Application Technology*, pp. 451-454, 2009.

[15] C. Duan, K. Zhang, and X.G. Wang, Dual Tree Complex Shearlet Transform and its Shift Invariance Properties, *Proc. of International Conference on Industrial Control and Electronics Engineering*, pp. 1800-1803, 2012.

[16] G. R. Easley, and D. Labate, Critically sampled wavelets with composite dilations, *IEEE Trans. Image Processing*, vol. 21, no. 2, pp. 550-561, 2012.

[17] N. Kingsbury, Complex wavelets for shift invariant analysis and filtering of signals, *Applied and computational harmonic analysis*, vol. 10, no. 3, pp. 234-253, 2001.

[18] N. Kingsbury, Image processing with complex wavelets, *Philosophical Transactions of the Royal Society of London A*, vol. 357, no. 1760, pp. 2543-2560, 1999.

[19] V. Petrovi, and C. Xydeas, On the effects of sensor noise in pixel-level image fusion performance, *Proc. of the 3rd International Conference on Information Fusion*, pp. WEC3/14-WEC3/19, 2000.

[20] R. Ghanem and P. D. Spanos, *Stochastic finite elements: a spectral approach, Revised Edition*, Springer, New York, USA, 2003.

[21] G. Piella, A general framework for multiresolution image fusion: from pixels to regions, *Information Fusion*, vol. 4, no. 4, pp. 259-280, 2003.

[22] Z. Wang, et al., A comparative analysis of image fusion methods, *IEEE Trans. Geoscience and Remote Sensing*, vol. 43, no. 6, pp. 1391-1402, 2005.

[23] G. Piella, and H. Heijmans, A new quality metric for image fusion, *Proc. of International Conference in Image Processing*, pp. III-173-6, 2003.

[24] Z. Wang, and A. C. Bovik, A universal image quality index, *IEEE Signal Processing Letters*, vol. 9, no. 3, pp. 81-84, 2002.